Cavity Ring-down Study of the Visible Absorption Spectrum of the Phenyl Radical and Kinetics of Its Reactions with Cl, Br, Cl_2, and O_2

K. Tonokura,* Y. Norikane, and M. Koshi

Department of Chemical System Engineering, School of Engineering, The University of Tokyo, 7-3-1 Hongo, Bunkyo-ku, Tokyo 113-8656, Japan

Y. Nakano, S. Nakamichi, M. Goto, S. Hashimoto, and M. Kawasaki

Department of Molecular Engineering, Kyoto University, Kyoto 606-8501, Japan

M. P. Sulbaek Andersen

University of S. Denmark, Department of Chemistry, Campusvej 55, DK-5230 Odense M, Denmark

M. D. Hurley and T. J. Wallington

Ford Motor Company, MD SRL3083, Dearborn, Michigan 48121-2053

Received: February 1, 2002; In Final Form: April 3, 2002

Cavity ring-down spectroscopy coupled with pulsed laser photolysis was used to study the visible absorption spectrum (490−535 nm, $^2B_1 \leftarrow {}^2A_1$ transition) of the phenyl radical, C_6H_5, in 10−50 Torr of argon diluent at 298 K. Absorption cross-sections were independent of total pressure over the range studied. At 504.8 nm, $\sigma_{phenyl} = (3.6 \pm 1.6) \times 10^{-19}$ cm^2 molecule^{-1} (base e). Spectral simulation of the rotational structure of an origin band was performed using a model for a type C vibronic band. The vibronic spectrum was analyzed using normal-mode information from quantum chemical calculations employing hybrid density functional theory (B3LYP/aug-cc-pVDZ). The a_1 and b_1 vibrations were confirmed in the vibronic spectrum. Cavity ring-down spectroscopy was used to follow the loss of phenyl radicals and measure $k(C_6H_5+Cl) = (1.2 \pm 0.8) \times 10^{-10}$, $k(C_6H_5+Br) = (7.0 \pm 4.0) \times 10^{-11}$, and $k(C_6H_5+Cl_2) = (2.96 \pm 0.53) \times 10^{-11}$ at 298K, and $k(C_6H_5+Cl_2) = (1.0^{+3.4}_{-0.5}) \times 10^{-12}$ exp[(1000 ± 470)/T] cm^3 molecule^{-1} s^{-1}. Relative rate techniques were used to measure $k(C_6H_5+Cl_2)/k(C_6H_5+O_2) = 2.1 \pm 0.4$ in 10−700 Torr of N_2 diluent at 296K. Combining the absolute and relative rate data gives $k(C_6H_5+O_2) = (1.4 \pm 0.4) \times 10^{-11}$ cm^3 molecule^{-1} s^{-1}. In 1 atm of air C_6H_5 radicals have a lifetime of approximately 1.4×10^{-8} s with respect to reaction with O_2 to give $C_6H_5O_2$ radicals. Results are discussed with respect to the spectroscopy and reactivity of C_6H_5 radicals. Quoted uncertainties are 2 standard deviations from regression analyses.

1. Introduction

Aromatic compounds such as benzene, toluene, and the xylenes are high octane constituents of gasoline. Regular grade gasoline sold in the U.S., Europe, and Japan contains 20−35% aromatics while premium grades have 30−50% aromatic content.[1,2] Aromatic species are important components of automobile tailpipe exhaust and evaporative emissions and contribute to formation of ozone and secondary organic aerosol in urban air.[3] The phenyl radical (C_6H_5•) is an important intermediate in the atmospheric chemistry of aromatic compounds. In combustion systems the phenyl radical is involved in the formation of soot and polycyclic aromatic hydrocarbons (PAH).[4] Spectroscopic and kinetic data concerning phenyl radicals are needed to understand the formation of soot and PAH in combustion and predict the environmental impact of vehicle exhaust.

Recognition of the importance of phenyl radicals has led to numerous experimental and computational studies of its spectroscopy and kinetics. In a pioneering gas-phase flash photolysis study, Porter and Ward[5] established that phenyl radicals have weak absorption bands in the visible (440−530 nm) which are assigned to a $^2B_1 \leftarrow {}^2A_1$ transition resulting from a $n \leftarrow \pi$ excitation. Cerecek and Kongshang[6] observed the UV absorption (240−270 nm) of phenyl radicals in aqueous solution. Ikeda et al.[7] recorded the UV absorption spectrum (220−350 nm) in the gas phase. Preidel and Zellner[8] used absorption at 488 nm (Ar^+ laser) to study the kinetics of phenyl radical reactions. Gunion et al.[9] conducted an ultraviolet photoelectron spectroscopy study of the phenide and observed the excited state of the phenyl radical at ≤1.7 eV (729 nm). Lin and co-workers[10] measured the absorption spectrum over the range 495−530 nm and conducted extensive kinetic studies of the phenyl radical.[10−16] Wallington et al.[17] studied the UV−vis (225−575 nm) absorption spectrum. The IR, visible, and UV absorption spectra of phenyl radicals in low-temperature argon matrixes have been the subject of several experimental investigations.[18−23] The geometric and electronic structure of the ground and lower excited states of the phenyl radical have been the subject of ab initio studies.[24−26]

Despite numerous studies, significant uncertainties remain in our understanding of the spectroscopy and kinetics of the phenyl radical. For example, the absolute strength of the visible

* Corresponding author. E-mail: tonokura@reac.t.u-tokyo.ac.jp.

10.1021/jp025585t CCC: $22.00
Published on Web 05/29/2002

absorption spectrum is unknown, and reported measurements of the rate constant for reaction 1 at ambient temperature range over 6 orders of magnitude from $k_1 < 2 \times 10^{-17}$[8] to $k_1 = (1.8 \pm 0.1) \times 10^{-11}$ cm^3 molecule^{-1} s^{-1}.[10]

$$C_6H_5 + O_2 + M \rightarrow C_6H_5O_2 + M \qquad (1)$$

To improve our understanding of phenyl radical chemistry we conducted a collaborative study in our laboratories. Three sets of experiments were performed. First, cavity ring-down spectroscopy (CRDS)[27] was employed at the University of Tokyo to provide the first absolute absorption spectrum of the phenyl radical in the visible region and kinetic data for the reaction of phenyl radicals with Cl and Br atoms. Quantum chemical calculations were performed to support the spectroscopic work. Second, CRDS was used at Kyoto University to study the kinetics of the reaction of phenyl radicals with Cl_2 (using spectral data from the University of Tokyo). Third, relative rate methods were employed at Ford Motor Company to determine the reactivity of phenyl radicals toward O_2.

2. Experimental Procedure

2.1. CRDS System at the University of Tokyo. Experiments were carried out using CRDS coupled with pulsed laser photolysis in a flow reactor described in detail elsewhere.[28] The ring-down cavity was 0.625 m long and consisted of a pair of high reflectance mirrors (Los Gatos Research, $R > 0.9999$ at 520 nm), with a 6 m radius of curvature, a diameter of 20 mm, and a usable bandwidth of approximately ±30 nm).

Phenyl radicals were generated by pulsed ArF excimer laser (193.3 nm, Lambda Physik COMPex 110) photolysis of C_6H_5-Cl or C_6H_5Br. The photolysis laser power was 1−10 mJ cm^{-2} per pulse. The average photon flux across the entire sample was uniform within 10%. The output of an excimer pumped dye laser (Lambda Physik LPX 110 + Lambda Physik LPD 3002, <10 μJ pulse^{-1}) was used for the probe laser. The photolysis laser entered the flow cell at right angles to the cavity and overlapped the probe laser beam at the center of the flow cell. The probe laser was injected through one of the mirrors into the ring down cavity. The decay of photon intensity within the cavity was measured by monitoring leakage of light through one of the cavity mirrors using a photomultiplier tube (PMT; Hamamatsu R955). The output of the signal from the PMT was fed to a 500 MHz, 1 GS/s digital oscilloscope (Tektronix TDS 520C) and transferred to a personal computer (PC) via a general purpose-interface bus. Typically, ring-down waveforms were averaged over 25 laser shots for each spectral point before being transferred to the PC.

The photon intensity decay rate in the cavity, β, was obtained by fitting the ring-down waveform to a single-exponential decay function and converted to the absorbance $\langle A \rangle$ via the following equation:[28]

$$\langle A \rangle = (l/c)(\langle \beta_{abs} \rangle - \langle \beta_{base} \rangle)$$

where l is the optical cavity length, c is the speed of light, $\langle \beta_{abs} \rangle$ is decay rate in the presence of an absorbing species, and $\langle \beta_{base} \rangle$ is the decay rate in the absence of the absorbing species. Absorption spectra were obtained by scanning the wavelength of the probe laser with a spectral resolution of 0.2 cm^{-1}. For time dependent studies, the delay time between the photolysis and probe laser beams was controlled by a pulse generator (Stanford Research Systems DG535).

Gas flows were regulated by calibrated mass flow controllers (Kofloc 3650). To protect the mirrors and photolysis beam entrance windows from deposition of reaction products, a slow flow of Ar (Nippon Sanso, >99.9999%) was introduced over these optical parts. C_6H_5Cl (Aldrich, 99.9%) and C_6H_5Br (Tokyo Kasei, >99%) were freeze−pump−thawed in liquid nitrogen to remove volatile contaminants and introduced into the reaction cell by passing a fraction of the argon diluent through a bubbler containing C_6H_5Cl or C_6H_5Br. The total pressure was measured at the center of the flow cell with a capacitance manometer (MKS Baratron 622A). Reagent concentrations were calculated from the total pressure, the calibrated flow rates, and the vapor pressure of the reagents. Spectroscopic and kinetic experiments were performed using a laser repetition of 1−10 Hz to ensure replenishment of the gas sample between successive laser shots. There was no discernible difference in the phenyl radical time profiles in experiments using N_2 and Ar buffer gases suggesting that diffusion from the viewing zone is not a significant factor in the phenyl radical loss. Experiments were performed at room temperature (298 ± 2 K).

2.2. CRDS System at Kyoto University. The cavity ring-down spectroscopy apparatus used at Kyoto University is described in detail elsewhere.[29] The system employs two pulsed lasers. The first laser (266-nm or 355-nm output of Nd^{3+}: YAG laser, Spectra Physics GCR-250) was used to photolyze a suitable precursor to generate phenyl radicals or Cl atoms. The second laser (Spectra Physics, PDL-3; Coumarin503, pumped by the 355-nm output of a Nd:YAG laser Quantel Brilliant) was used to probe absorption of the phenyl radical. After the photolysis laser beam traversed the cell nearly collinear to the axis of the ring-down cavity, the probe laser beam was injected through one of two high-reflectivity mirrors which made up the ring-down cavity. The mirrors (Research Electro Optics) had a specified maximum reflectivity of 0.9985 at 514 nm, a diameter of 7.8 mm, a radius of curvature of 1 m, and were mounted 1.04 m apart. Light leaking from one of the mirrors of the ring-down cavity was detected by a gated photomultiplier tube (Hamamatsu: C1392−56/R212UH) through a narrow band-pass filter (Edmund Industrial Optics Co., central wavelength: 505 nm, fwhm: ±1.5 nm). The decay of the light intensity was recorded using a digital oscilloscope (Tektronix TDS430A) and transferred to a personal computer. The decay of the light intensity is given by the expression:

$$I(t) = I_0 \exp(-t/\tau) = I_0 \exp(-t/\tau_0 - \sigma nc(L_R/L)t)$$

where I_0 and $I(t)$ are the intensities of light at time 0 and t, respectively. τ_0 is the empty cavity ring-down time (2 μs at 514 nm). L_R is the length of the reaction region (0.55 m). L is the cavity length (1.04 m). τ is the measured cavity ring-down time. n and σ are the concentration and absorption cross section of the species of interest, and c is the velocity of light.

The reaction cell consisted of a Pyrex glass tube (21 mm i.d.), which was evacuated by a combination of an oil rotary pump and a mechanical booster pump. The temperature of the gas flow region was controlled by circulation of a thermostated mixture of ethylene glycol and water and was controllable over the range 280−330 K. The difference between the temperature of sample gas at the entrance and exit of the flow region was <1 K. The pressure in the cell was monitored by an absolute pressure gauge (Baratron). Gas flows were measured and regulated by mass flow controllers (Kofloc 3650). A slow flow of nitrogen diluent gas was introduced at both ends of the ring-down cavity close to the mirrors to minimize deterioration caused by exposure to reactants and products. The total flow rate was kept constant at 3.5×10^2 cm^3 min^{-1} (STP). Nitrosobenzene (C_6H_5NO) was used as the photolytic precursor

for phenyl radicals and was introduced to the reaction tube by passing N_2 diluent gas over solid C_6H_5NO. The concentration of C_6H_5NO was measured downstream of the reaction tube by monitoring the absorption at 253.7 nm ($\sigma = 6.86 \times 10^{-18}$ cm^2 molecule^{-1} [30]). Other reagent concentrations were calculated from the flow rates and total pressure. Kinetic experiments were performed using a laser repetition of 1 Hz. All reagents were obtained from commercial sources. C_6H_5NO (97%), N_2 (> 99.999%), and Cl_2 (99.9%) were used without further purification.

2.3. FTIR Smog Chamber System at Ford. Experiments were performed in a 140 L Pyrex reactor interfaced to a Mattson Sirus 100 FTIR spectrometer.[31] The optical path length of the infrared beam was 27 m. The reactor was surrounded by 22 fluorescent blacklamps (GE F15T8-BL) which were used to photochemically initiate the experiments by photolysis of Cl_2. The loss of benzaldehyde and formation of benzoyl chloride, chlorobenzene, and CO_2, were monitored by Fourier transform infrared (FTIR) spectroscopy using a spectral resolution of 0.25 cm^{-1}. IR spectra were derived from 32 coadded interferograms. Reference spectra were acquired by expanding known volumes of reference materials into the chamber. Products were identified and quantified by fitting reference spectra of the pure compounds to the observed product spectra using integrated absorption features over the following wavenumber ranges (cm^{-1}): 790−850 (C_6H_5CHO), 750−780 ($C_6H_5C(O)Cl$), 720−760 (C_6H_5Cl), and 2300−2400 (CO_2).

Experimental conditions for the kinetic study were 9.8−10.2 mTorr of C_6H_5CHO, 224−890 mTorr of Cl_2, and 2.4−9.2 Torr of O_2 in 10, 100, or 700 Torr of N_2 diluent. All experiments were performed at 296 ± 2 K. Reagents were obtained from commercial sources at purities > 99%. Samples of C_6H_5CHO, C_6H_5Cl, and $C_6H_5C(O)Cl$ were subjected to repeated freeze−pump−thaw cycling before use. In smog chamber experiments it is important to check for unwanted loss of reactants and products via photolysis, dark chemistry and heterogeneous reactions. Control experiments were performed in which mixtures of C_6H_5CHO, C_6H_5Cl, and $C_6H_5C(O)Cl$ in air were subjected to UV irradiation for 15 min and product mixtures obtained after the UV irradiation of $C_6H_5CHO/O_2/Cl_2/N_2$ mixtures were allowed to stand in the dark in the chamber for 15 min. There was no observable loss of reactants or products suggesting that photolysis, and heterogeneous reactions are not a significant complication in the present work.

3. Results and Discussion

3.1. Absorption Spectrum and Molecular Structure. The equilibrium geometries of the ground and excited states of the phenyl radical were optimized employing a hybrid density function theory B3LYP, based on Becke's three-grid integration[32] and exchange functional and the correction functional of Lee, Yang, and Parr,[33] with Dunning's correction consistent aug-cc-pVDZ basis set.[34] Vibrational frequencies of the ground and excited states were also calculated at the B3LYP/aug-cc-pVDZ method. The systems were restricted to C_{2v} symmetry in the optimization. Calculations were carried out using the Gaussian 98 suite of programs.[35] The optimized geometries of the $^2A_1$ ground and $^2B_1$ excited states are shown in Figure 1.

Figure 2 shows the absorption spectrum of the phenyl radical in the spectral region between 490 and 535 nm produced in the 193.3 nm photolysis of chlorobenzene. The same absorption spectrum was observed following 193.3 nm photolysis of bromobenzene. The absorption spectrum exhibits no fine structure within the probe laser bandwidth ($\Delta\nu = 0.2$ cm^{-1})

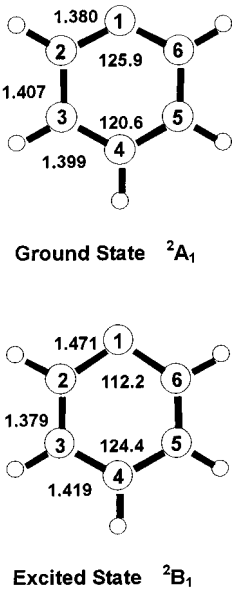

Figure 1. Molecular structures of the phenyl radical in the ground and first excited states optimized at the B3LYP/aug-cc-PVDZ level of theory.

and no dependence on total pressure (10−50 Torr). As the delay time between the photolysis laser and probe laser was increased to a few milliseconds, the spectral bands decayed and vanished, thus establishing the transient nature of the spectral carrier. Plots of absorbance versus photolysis laser power had a slope of 0.9 ± 0.1 indicating that the absorbing species is formed in a one-photon process. Multiphoton excitation of the parent molecule and secondary photodissociation of primary products are not significant. The small absorption bands labeled with asterisks in Figure 2 decayed more rapidly than the other features and are assigned to hot bands. Relaxation of vibrationally excited hydrocarbon radicals by collisions with argon typically occurs with deactivation rate constants of the order of 10^{-13} cm^3 molecule^{-1} s^{-1}.[36] The relaxation time of the hot bands in 40 Torr of argon diluent was approximately 10 μs, consistent with that expected for vibrationally excited hydrocarbon radicals. The peak positions in the spectrum agree with the electronic absorption spectrum ascribed to a $^2B_1 \leftarrow {}^2A_1$ transition of the phenyl radical[19] with a band origin at 18908 cm^{-1} reported by Porter and Ward.[5] The absolute values of vertical axis of Figure 2 (i.e., absorption cross section) were determined through the analysis of the time profiles of absorption peak at 504.8 nm. The details are described in the section 3.2.

Spectral band simulations were performed with the FRASY-ROT program.[37] Figure 3 shows both the experimental spectrum and the simulated spectrum of the band envelope. Taking a coordinate system in which a planar radical lies in the *yz* plane and the C_2 axis is the *z* axis, a transition moment oriented along the *x*, *y*, and *z* axes gives type C, A, and B bands, which corresponds to B_1, B_2, and A_1 vibronic symmetries, respectively, for the upper states. Since the vibronic symmetry of the ground state is A_1 and the excited state is B_1, parity selection rules allow only type C band of an oblate symmetric top (asymmetry parameter $\kappa \approx 0.6$ for the $^2A_1$ ground state, $\kappa \approx 0.8$ for the $^2B_1$ excited state). The $^2B_1 \leftarrow {}^2A_1$ electronic transition involves promotion of an electron from an out-of-plane π-bonding orbital, parallel to the out-of-plane *c* axis, into an in-plane, nonbonding orbital, and the transition moment is perpendicular to the plane of the ring. The rotational selection rules are $\Delta K_a = \pm 1$, $\Delta K_c = 0$, and $\Delta J = 0, \pm 1$. The rotational constants for the ground

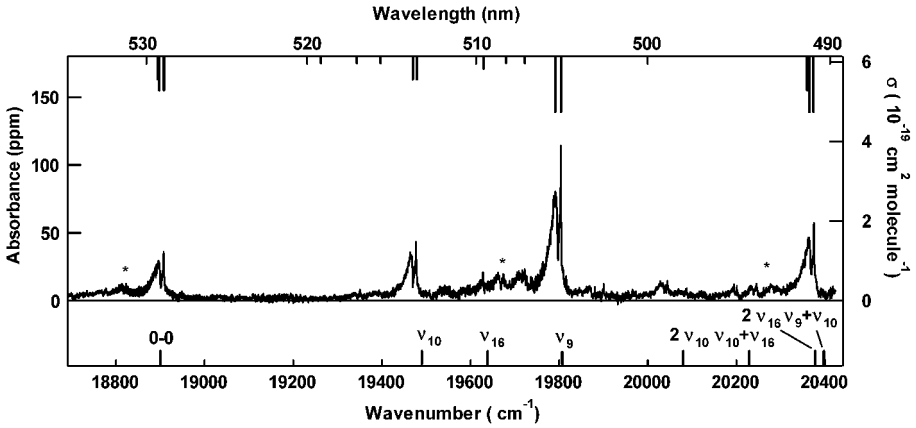

Figure 2. Absorption spectrum of the phenyl radical observed from the 193.3 nm photolysis of chlorobenzene. The time delay between the photolysis and probe laser beams was 1 μs. The starred features in the experimental spectrum are hot bands. The upper stick spectrum shows the positions and relative intensities of the phenyl radical absorption peaks by Porter and Ward.[5] The lower stick spectrum indicates the vibrational bands at $^2B_1$ state.

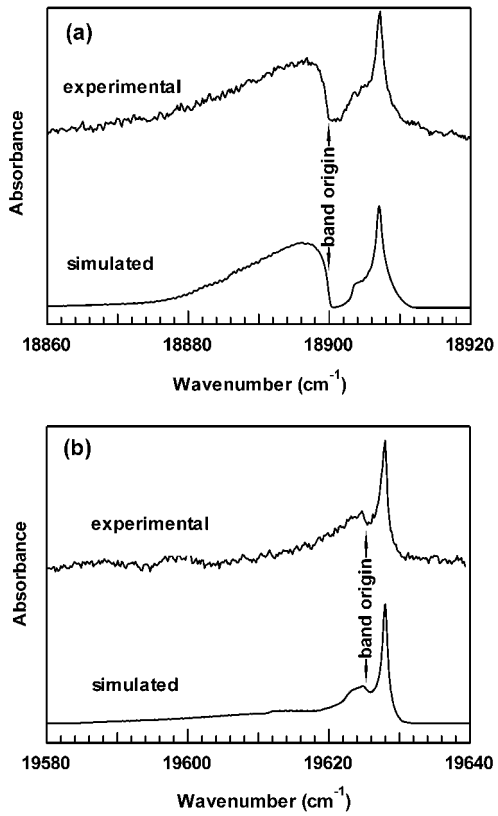

Figure 3. The upper curve is the measured band-origin spectrum, the lower curve is the spectrum simulated (a) C type and (b) B type band of an oblate asymmetric top with molecular constants calculated with the B3LYP/aug-cc-pVDZ method.

and excited states were calculated from the planar B3LYP aug-/cc-pVDZ geometries (Table 1), neglecting centrifugal distortion and spin-rotation effects. In the simulation, a 298 K rotational temperature is assumed and the final contour was obtained by convoluting the calculated stick spectrum with a 0.5 cm^{-1} Lorentzian line shape. The unresolved rotational structure of the origin band observed experimentally is well reproduced by the calculations. The sharp peak at 18908 cm^{-1} corresponds to a R-branch bandhead, Q- and P-branches produce a broad feature to the red of the band maximum. The band origin derived from the simulation as the type C band is $T_0 = 18900$ cm^{-1}.[38] The agreement between the experimental spectrum and the simulated spectrum is evidence that the C_{2v} symmetry is held in the $^2B_1$ state.

The equilibrium geometries calculated at B3LYP/aug-cc-pVDZ level for the $^2A_1$ ground state and $^2B_1$ excited state exhibit C_{2v} symmetric structure (Figure 1). The $C_2-C_1-C_6$ bond angle decreases from 125.9° for the ground state to 112.2° in the excited state. The C_1-C_2 and C_1-C_6 bonds lengthen from 1.380 Å for the ground state to 1.471 Å for the excited state. The structural changes are due to the reduction of a C−C π-bonding population, resulting from removal of one electron from the π system to a σ orbital hole. Vibrational frequencies and rotational constants of the ground and first excited states, calculated at B3LYP/aug-cc-pVDZ level are presented in Table 1. The mean absolute deviation of the B3LYP/aug-cc-pVDZ calculated from the experimental frequencies[20] of the phenyl radical in the ground state in Ar matrix is 2.6%. Gunion et al.[9] observed two gas phase a_1 vibrations of the phenyl radical in a photodetachment study. In the excited state, the vibrational frequencies change substantially. Most in-plane a_1 normal modes decrease their frequencies in the excited state. For instance, the ν_9 frequency of the $C_2-C_1-C_6$ bending mode decreases from 979 to 907 cm^{-1}. This frequency change is caused by the in-plane distortion in the excited state. Since the $C_2-C_1-C_6$ angle decreases in the excited state, the C−C−C bending mode would be prominent in the absorption spectrum. Porter and Ward[5] derived fundamental frequencies of 571, 722, and 896 cm^{-1} from their visible absorption spectrum. These bands are assigned to $C_1-C_{2,6}$ and $C_4-C_{3,5}$ bending (ν_{10}, a_1), $C_{2,3,4,5,6}-H$ bending (ν_{16}, b_1), and C−C−C bending and C−H bending (ν_9, a_1) modes, with the values obtained in the present calculations of 584, 736, and 907 cm^{-1}, respectively. The progressions in the spectrum are indicated in Figure 2 and Table 1. The spectral shapes of ν_9 and ν_{10} bands show the same shape with the origin band as the type C band (B_1 vibronic symmetry). On the other hand, the ν_{16} band is identified to A_1 vibronic symmetry, because the direct product b_1 (ν_{16}) ⊗ B_1 ($^2B_1$) gives the A_1 irreducible representation. The rotational simulation at this band was performed by its rotational contour as type B band, which reproduces well the experimental band structure (see Figure 3). The results of the spectral simulation using calculated molecular parameters confirm the finding of Radziszewski[19] that the visible absorption of the phenyl radical corresponds to the $^2B_1 \leftarrow {}^2A_1$ transition. The observed vibronic components are A_1 and B_1 symmetry, which means that b_1 and a_1 vibrations participate in the progression.

3.2. Cavity Ring-down Study of $k(C_6H_5+Cl)$, $k(C_6H_5+Br)$, and $\sigma(C_6H_5)$. Parts a and b of Figure 4 show the transient absorption at 504.8 nm observed as a function of time following

TABLE 1: Vibrational Frequencies (cm^{-1}) and Rotational Constants (cm^{-1}) of the Phenyl Radical

			$^2A_1$			$^2B_1$	
ν_i	sym	assignment[a]	B3LYP	exptl[b]	exptl[c]	B3LYP	exptl[d]
1	a_1	C−H sym s (C_4H predominantly)	3198	3085		3188	
2		$C_{2,6}$−H sym s, oop C_4−H s	3185	3071		3161	
3		$C_{2,4,6}$−H sym s, oop C_4−H s	3167	3052		3138	
4		$C_{2,6}$−C-$_{3,5}$ sym s, $C_{3,5}$−H ip b	1572	1499		1600	
5		C_1−$C_{2,6}$ sym s, $C_{2,3,5,6}$−H ip b	1458	1441		1426	
6		$C_{2,3,5,6}$−H b	1166	1080		1202	
7		C_1−$C_{2,6}$ s, $C_{2,3,5,6}$−H ip b	1046	1027		1007	
8		ring breathing mode	1017	1011		993	
9		C−C−C b, C−H b	979	976	968	907	896
10		C_1−$C_{2,6}$, C_4−$C_{3,5}$ b	615	605	600	584	571
11	a_2	$C_{2,5}$−H oop $C_{4,6}$−H b	958			984	
12		$C_{2,3}$−H oop $C_{5,6}$−H b	807			782	
13		$C_{2,4}$−H oop $C_{3,6}$−H b	400			268	
14	b_1	$C_{2,4,6}$−H oop $C_{3,5}$−H b	985	971		1015	
15		$C_{2,4,6}$−H b	885	878		941	
16		C−H b	714	708		736	726
17		$C_{2,4,6}$−H b	670	629		660	
18		$C_{2,3,5,6}$−H oop C_4−H b	423	416		343	
19	b_2	$C_{2,3}$−H s $C_{5,6}$−H as s	3187	3073		3165	
20		$C_{2,5}$−H sym s oop $C_{3,6}$−H sym s	3172	3060		3139	
21		$C_{1,2}$−$C_{4,5}$ sym s oop $C_{3,6}$−H b	1629	1593		1515	
22		C−C s $C_{3,4,5}$−H b	1450	1433		1378	
23		Kekule mode $C_{3,5}$−H ip b	1333	1344		1332	
24		$C_{2,3}$−$C_{5,6}$ s oop C−H b	1293	1226		1239	
25		$C_{3,4,5}$−H ip b	1166	1086		1101	
26		C_2−C_3s oop C_5−C_6 s $C_{2,4,6}$−H oop b	1069	1067		1043	
27		ring s	596	586		515	
rotational constant (cm^{-1})							
		A	0.2085			0.1964	
		B	0.1860			0.1846	
		C	0.0983			0.0952	

[a] s = stretch, sym = symmetric, as = asymmetric, b = bend, ip = in-phase, oop = out-of-phase. [b] Reference 20. In Ar matrix. [c] Reference 9. Gas-phase experimental values.

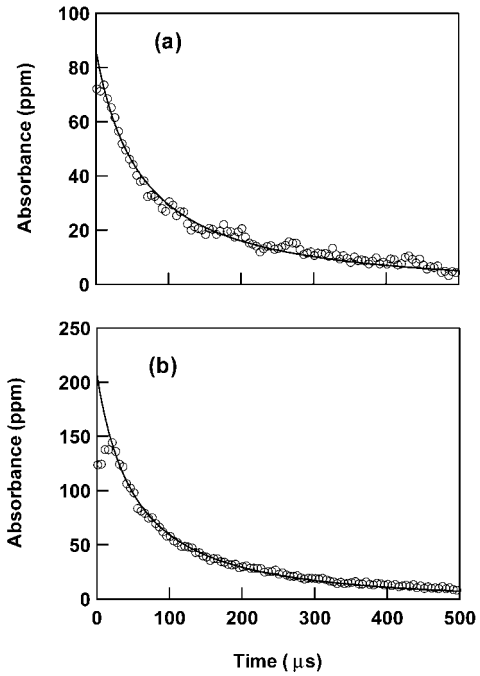

Figure 4. Absorbance at 504.8 nm by phenyl radicals following the 193.3 nm photolysis of (a) chlorobenzene (2.0×10^{15} molecules cm^{-3}) and (b) bromobenzene (4.7×10^{14} molecules cm^{-3}) in 40 Torr of argon diluent versus the time delay between photolysis and probe laser. The solid curves are fits to the data (see text for details).

the 193.3 nm photolysis of mixtures containing either 2.0×10^{15} molecules cm^{-3} C_6H_5Cl or 4.7×10^{14} molecules cm^{-3} C_6H_5Br in 40 Torr of argon diluent at 298 K. As discussed in section 3.1, the absorption at 504.8 nm is attributable to phenyl radicals formed by the photodissociation of C_6H_5X (X = Cl and Br). The small initial rise in absorption in part 4b and the slight delay in the decay of absorption evident by close inspection of part 4a occur on a time scale which is indistinguishable from that of relaxation of the hot bands described in section 3.1. It seems reasonable to conclude that the small increase in absorption at times up to 40 μs after photolysis reflects the relaxation of hot phenyl radicals produced by the photodissociation.

The transient absorption profiles in Figure 4 can be used to extract information concerning the absorption cross section and reaction kinetics of phenyl radicals.[28] The phenyl radical quantum yield following the 193.3 nm photoexcitation of C_6H_5-Cl or C_6H_5Br is essentially unity.[39] Photolysis of C_6H_5X gives rise to equal concentrations of phenyl radicals and halogen atoms which can then undergo self-reaction, cross reaction, and reaction with C_6H_5X.

$$C_6H_5X + h\nu(\lambda{=}193.3\text{ nm}) \rightarrow C_6H_5 + X, \quad X = \text{Cl and Br} \tag{2}$$

$$C_6H_5 + C_6H_5 \rightarrow \text{products} \tag{3}$$

$$C_6H_5 + X \rightarrow \text{products} \tag{4}$$

$$C_6H_5 + C_6H_5X \rightarrow \text{products} \tag{5}$$

$$X + X \rightarrow X_2 \tag{6}$$

$$X + C_6H_5X \rightarrow \text{products} \tag{7}$$

Under the present experimental conditions, the loss of C_6H_5 radicals and X atoms by diffusion or flow from the viewing region is too slow ($<100\ s^{-1}$) relative to the experimental time scale (see Figure 4) to have any significant impact. Phenyl radicals react very slowly (rate constants of the order of 10^{-16}

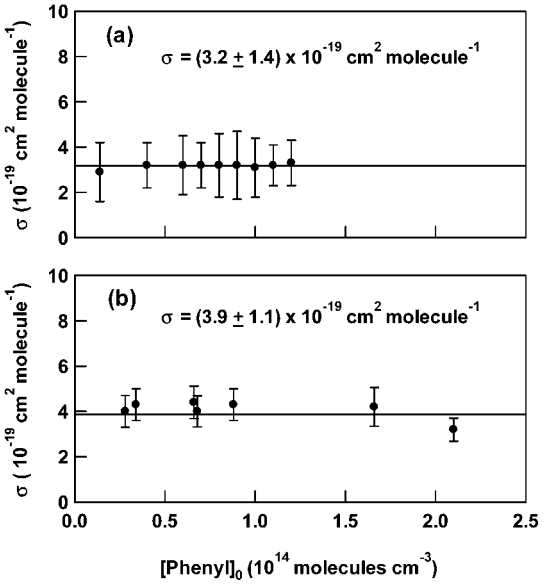

Figure 5. Plots of calculated absorption cross-section at 504.8 nm as a function of $[C_6H_5]_o$ in experiments using $(4-12) \times 10^{14}$ molecules cm^{-3} of chlorobenzene (top part) or $(2-5) \times 10^{14}$ molecules cm^{-3} of bromobenzene (bottom part) with laser photolysis energies of 0.8−7.5 mJ cm^{-2} $pulse^{-1}$.

cm^3 $molecule^{-1}$ s^{-1} at 298 K[40−42]) with aromatic compounds such as C_6H_5Cl and C_6H_5Br; reaction 5 is not important in the present work. Recombination of Cl and Br atoms via reaction 6 in 40 Torr of argon diluent proceeds slowly (pseudo-second-order rate constants of approximately 10^{-14} cm^3 $molecule^{-1}$ s^{-1} [43]); reaction 6 is not important over the time scale of the present experiments (0−500 μs, see Figure 4). Reaction of Cl atoms with C_6H_5Cl proceeds with a rate constant $< 2.5 \times 10^{-16}$ cm^3 $molecule^{-1}$ s^{-1},[44] and it is likely that reaction of Br atoms with C_6H_5Br is equally slow: reaction 7 is not significant in the present work. We conclude that the loss of C_6H_5 radicals evident in Figure 4 is determined by reactions 3 and 4. The kinetics of reaction 3 are well established; $k_3 = (1.9 \pm 0.2) \times 10^{-11}$ cm^3 $molecule^{-1}$ s^{-1}.[45] There are no available data concerning reaction 4.

To derive values for k_4 and σ(504.8 nm) the observed phenyl radical decays such as those shown in Figure 4 were modeled using a simple kinetic mechanism consisting of reactions 3 and 4. The coupled differential equations describing the loss of C_6H_5 radicals and X atoms in the system were solved by numerical integration routines.[28] Three parameters were varied simultaneously to provide the best fit; $[C_6H_5]_o = [X]_o$, k_4, and σ(504.8 nm). The curves in Figure 4 are fits to the data which show that the simple model provides a good description of the experimental observations. Experiments employing C_6H_5Cl photolysis gave values of $k(C_6H_5 + Cl) = (1.2 \pm 0.8) \times 10^{-10}$ cm^3 $molecule^{-1}$ s^{-1} and σ(504.8 nm) $= (3.2 \pm 1.4) \times 10^{-19}$ cm^2 $molecule^{-1}$. Experiments employing C_6H_5Br photolysis gave values of $k(C_6H_5 + Br) = (7.0 \pm 4.0) \times 10^{-11}$ cm^3 $molecule^{-1}$ s^{-1} and σ(504.8 nm) $= (3.9 \pm 1.1) \times 10^{-19}$ cm^2 $molecule^{-1}$. The values of σ(504.8 nm) derived from experiments employing C_6H_5Cl and C_6H_5Br photolysis were indistinguishable within the experimental uncertainties. Variation of the initial radical concentration by an order of magnitude had no discernible impact on the values of k_4 or σ(504.8 nm) (see Figure 5) returned from the fitting procedure. We choose to quote a final value of σ(504.8 nm) which is the average of the two determinations with errors limits which encompass the extremes of the determinations; hence, σ (504.8 nm) $= (3.6 \pm 1.6) \times 10^{-19}$ cm^2 $molecule^{-1}$.

A value of σ (504.8 nm) can also be derived using the relationships

$$[C_6H_5]_0 = N_p[C_6H_5X]\sigma^{193}_{C_6H_5X}\phi$$

$$\langle A\rangle_0 = \sigma_{C_6H_5}[C_6H_5]_0 l_s$$

N_p is the laser photon number density (determined from laser pulse energy measurements). $[C_6H_5X]$ is the phenyl precursor concentration. $\sigma_{C_6H_5X}$ is the absorption cross section at 193.3 nm ($\sigma_{C_6H_5Cl} = 2.5 \times 10^{-17}$,[46] $\sigma_{C_6H_5Br} = 4.7 \times 10^{-17}$ cm^2 $molecule^{-1}$ [measured during the present work]). ϕ is the phenyl radical quantum yield (assumed to be unity). $\langle A\rangle_0$ is the absorption extrapolated to zero time after the photolysis pulse. l_s is absorption path length (∼30 mm) induced by the photolysis laser beam. Using this approach a value of σ (504.8 nm) $= (2.5 \pm 0.5) \times 10^{-19}$ cm^2 $molecule^{-1}$ was derived. It is gratifying that values of σ (504.8 nm) obtained using the two different approaches are indistinguishable within the experimental uncertainties. In view of the potential systematic uncertainties associated with estimation of the photolysis laser flux and C_6H_5X concentration within the reaction cell we prefer the value of σ (504.8 nm) $= (3.6 \pm 1.6) \times 10^{-19}$ cm^2 $molecule^{-1}$ derived from fits to the phenyl radical decay.

The absorption cross section data from the present work can be compared to two previous gas-phase measurements; σ (488 nm) $= (9 \pm 4) \times 10^{-19}$ cm^2 $molecule^{-1}$ by Preidel and Zellner[8] and σ (504.8 nm) $< 5 \times 10^{-19}$ cm^2 $molecule^{-1}$ by Wallington et al.[17] Preidel and Zellner assumed that absorption they observed at 488 nm was due to the rotational structure of the vibrational band and pressure broadening of the nearby absorption band. However, no absorption at 488 nm was observed in the present study. Wallington et al.[17] deduced that the results of Preidel and Zellner gives σ (504.8 nm) $= (4.5 \pm 2) \times 10^{-18}$ cm^2 $molecule^{-1}$ and concluded that at the monitoring wavelength employed by Preidel and Zellner there was substantial interference by one or more absorption transient species other than phenyl radicals. The present work supports this conclusion. The upper limit of $\sigma_{C_6H_5}$(504.8 nm) $< 5 \times 10^{-19}$ cm^2 $molecule^{-1}$ reported by Wallington et al.[17] is consistent with the value measured in the present work; σ (504.8 nm) $= (3.6 \pm 1.6) \times 10^{-19}$ cm^2 $molecule^{-1}$.

Radziszewski[19] studied the UV and visible absorption of phenyl radicals in low temperature (6 K) argon matrixes and estimated an absorption cross section for the origin band of $\sigma_{C_6H_5}$ (510.5 nm) $= 1.1 \times 10^{-20}$ cm^2 $molecule^{-1}$. This result is approximately 30 times less than the value measured in the gas phase in the present work; σ (504.8 nm) $= (3.6 \pm 1.6) \times 10^{-19}$ cm^2 $molecule^{-1}$. Interestingly, the cross section reported by Radziszewski[19] at the maximum of the UV absorption band, σ (235.1 nm) $= 8.4 \times 10^{-19}$ cm^2 $molecule^{-1}$, is approximately a factor of 40 times less than that observed in the gas phase; σ (240 nm) $= 3.6 \times 10^{-17}$ cm^2 $molecule^{-1}$.[17] The UV−vis absorption observed in low-temperature argon matrixes by Radziszewski[19] appears to be uniformly 30−40 times less intense than that observed in the gas phase. The UV−vis absorption of species in low temperature argon matrixes is usually comparable to that observed in the gas phase and it is difficult to understand why the spectrum of Radziszewski[19] is a factor of 30−40 times less intense than that measured herein.

3.3. Cavity Ring-down Study of $k(C_6H_5+Cl_2)$. The kinetics of the reaction of phenyl radicals with molecular chlorine were

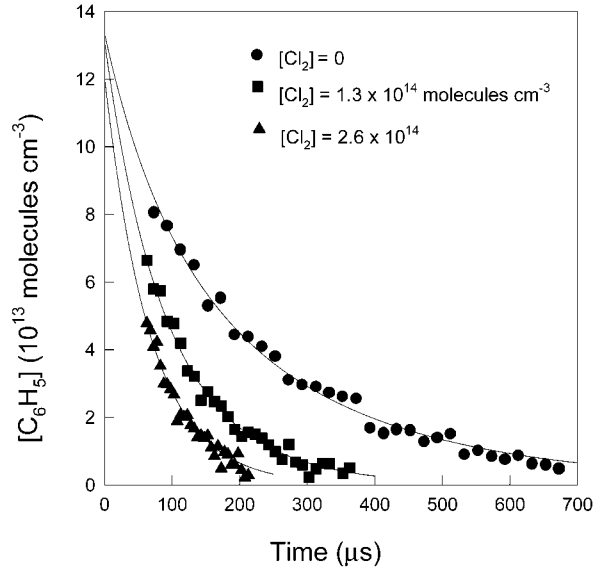

Figure 6. Decay of absorption at 504.8 nm as a function of time following the 266 nm photolysis of C_6H_5NO in the presence of different concentrations of Cl_2. The solid lines are fits to data.

studied at Kyoto University using CRDS. Phenyl radicals were produced by the 266 nm photolysis of C_6H_5NO ($1.8-3.9 \times 10^{14}$ molecules cm^{-3})[8] in 15 Torr of N_2 diluent at 280−330 K in the presence and absence of Cl_2 ($(0-5) \times 10^{14}$ molecules cm^{-3}). Using our absorption cross section for C_6H_5, σ (504.8 nm) = $(3.6 \pm 1.6) \times 10^{-19}$ cm^2 $molecule^{-1}$, the temporal decay curves of the absorbance at 504.8 nm were measured at various Cl_2 concentrations and temperatures (T = 280−330 K).

Figure 6 shows plots of the absorption at 504.8 nm following 266 nm photolysis of $C_6H_5NO/Cl_2/N_2$ mixtures with $[Cl_2]$ 0, 1.3×10^{14}, 2.6×10^{14} molecules cm^{-3} at 300 K. Under these conditions, there are five possible chemical loss mechanisms for phenyl radicals in the system:[13,45]

$$C_6H_5 + Cl_2 \rightarrow C_6H_5Cl + Cl \quad (8)$$

$$C_6H_5 + C_6H_5NO \rightarrow (C_6H_5)_2NO \quad (9)$$

$$C_6H_5 + C_6H_5 \rightarrow (C_6H_5)_2 \quad (3)$$

$$C_6H_5 + NO \rightarrow C_6H_5NO \quad (10)$$

$$C_6H_5 + Cl \rightarrow \text{products} \quad (11)$$

where the rate constants of those reactions are reported to be k_9 = $(8.14 \pm 0.33) \times 10^{-12}$ exp[(34 ± 16)/T] cm^3 $molecule^{-1}$ s^{-1},[45] k_3 = $(2.31 \pm 0.18) \times 10^{-11}$exp[$(56 \pm 36)$/T] cm^3 $molecule^{-1}$ s^{-1},[45] k_{10} = 4.47×10^{-12} exp[(433 ± 111)/T] cm^3 $molecule^{-1}$ s^{-1},[13] and our rate constant of reaction 11: k_{11} = $(1.2 \pm 0.4) \times 10^{-10}$ cm^3 $molecule^{-1}$ s^{-1} (assumed to be temperature independent). The observed decay of phenyl radicals was simulated using a model consisting of reactions 3 and 8−11, with k_8 adjusted to give the best fit (shown by solid curves in Figure 6). The result of the fitting procedure gave k_8 = $(2.96 \pm 0.53) \times 10^{-11}$ cm^3 $molecule^{-1}$ s^{-1} at 300 K.

The reaction of phenyl radicals with molecular chlorine generates Cl atoms which raises the possibility that phenyl radicals could be regenerated by reaction of Cl atoms with C_6H_5-NO.

$$Cl + C_6H_5NO \rightarrow C_6H_5 + NOCl \quad (12)$$

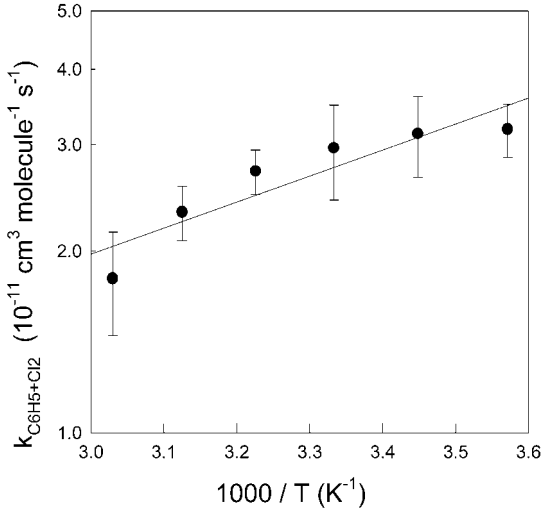

Figure 7. Arrhenius plot for $C_6H_5 + Cl_2$ reaction.

TABLE 2: Values of $k(C_6H_5 + Cl_2)$ Measured in the Present Work

temperature (K)	$k(C_6H_5 + Cl_2)$ (cm^3 $molecule^{-1}$ s^{-1})
280	$(3.18 \pm 0.32) \times 10^{-11}$
290	$(3.13 \pm 0.48) \times 10^{-11}$
300	$(2.96 \pm 0.53) \times 10^{-11}$
310	$(2.71 \pm 0.23) \times 10^{-11}$
320	$(2.32 \pm 0.24) \times 10^{-11}$
330	$(1.80 \pm 0.35) \times 10^{-11}$

To explore this possibility experiments were performed to quantify the generation of phenyl radicals following reaction of Cl atoms with C_6H_5NO. In these experiments Cl atoms were produced by the 355 nm photolysis of Cl_2 ($5-500 \times 10^{13}$ molecules cm^{-3}) in the presence of C_6H_5NO ($1-230 \times 10^{14}$ molecules cm^{-3}) at a total pressure of 15 Torr with N_2 diluent at 298 K. Evidence of phenyl radical formation was sought by monitoring at 504.8 nm. In these experiments there was no observable formation of phenyl radicals with our CRDS study (maximum detection limit is 5.6×10^{12} molecules cm^{-3}). We conclude that generation of phenyl radicals via reaction of Cl atoms with C_6H_5NO is not a significant complication in the present work. Using the detection limit for phenyl radicals (5.6×10^{12} molecules cm^{-3}), the photolysis laser photon number density (4.55×10^{17} photons cm^{-2}), the concentration of Cl_2 molecules (2.0×10^{15} molecules cm^{-3}) and C_6H_5NO (2.3×10^{16} molecules cm^{-3}), the absorption cross section of Cl_2 at 355 nm (σ_{Cl2} (300 K)= $1.57 \times 10^{-19}$$cm^2$ $molecule^{-1}$),[47] the Cl_2 photodissociation quantum yield at 355 nm (assumed to be unity), and the second-order decay rate constant of the reaction of phenyl radical with Cl_2 (2.96×10^{-11} cm^3 $molecule^{-1}$ s^{-1}), an upper limit value of $k_{12} < 1.0 \times 10^{-14}$ cm^3 $molecule^{-1}$ s^{-1} was determined.

To determine the Arrhenius expression for the reaction of phenyl radical with Cl_2, values of k_8 were determined at various temperatures over the range (280−330 K). The results are listed in Table 2 and plotted in Figure 7. The line through the data in Figure 7 is a fit of the Arrhenius expression to the data which gives k_8 = $(1.0^{+3.4}_{-0.5}) \times 10^{-12}$ exp[(1000 ± 470)/T] cm^3 $molecule^{-1}$ s^{-1}.

It can be argued that the data in Figure 7 suggest that the Arrhenius plot for reaction 8 is curved. For completeness, a modified Arrhenius expression with a temperature-dependent preexponential factor, $k = BT^n\exp(E_a/RT)$, was fit to the data in Figure 7. This analysis returned a value of n which was indistinguishable from zero. We conclude that the kinetics of

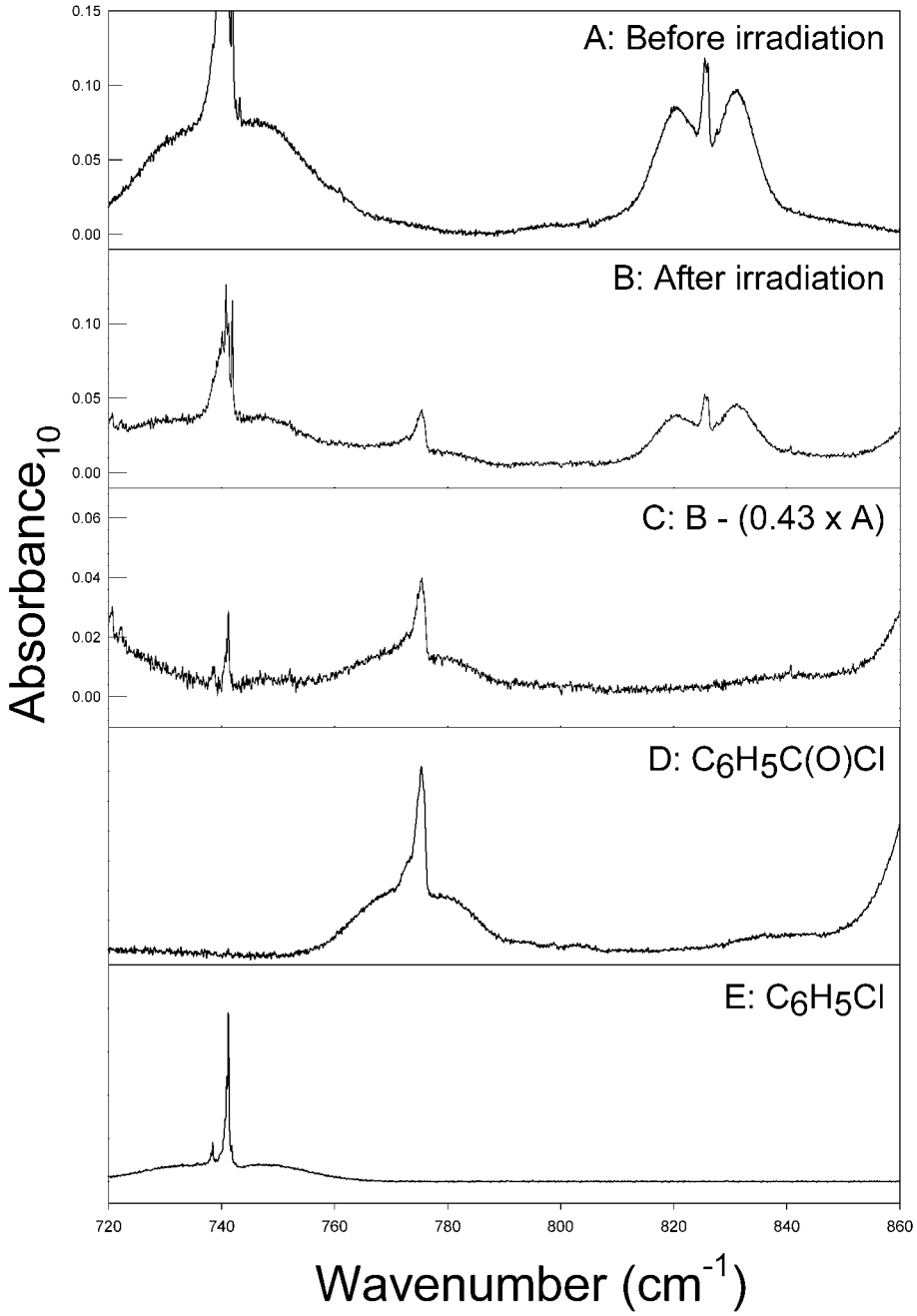

Figure 8. IR spectra obtained before (A) and after (B) a 7 s irradiation of a mixture of 9.92 mTorr C_6H_5CHO, 5.52 Torr O_2 and 557 mTorr Cl_2 in 700 Torr of N_2 at 296 K. Parts D and E are reference spectra of $C_6H_5C(O)Cl$ and C_6H_5Cl, respectively.

reaction 8 are adequately described by the simple Arrhenius expression $k_8 = (1.0^{+3.4}_{-0.5}) \times 10^{-12}$ exp[(1000 ± 470)/T] cm^3 molecule^{-1} s^{-1}. The negative activation energy suggests that the reaction of phenyl radicals with Cl_2 proceeds via an associated complex as shown below.

$$C_6H_5 + Cl_2 \rightarrow [C_6H_5{-}Cl_2] \rightarrow C_6H_5Cl + Cl \qquad (8)$$

3.4. Relative Rate Study of $k(C_6H_5+Cl_2)/k(C_6H_5+O_2)$. The rate constant ratio k_8/k_1 was measured using a FTIR smog chamber system at Ford by irradiating $C_6H_5CHO/O_2/Cl_2/N_2$ mixtures and observing the dependence of the C_6H_5Cl yield on the concentration ratio $[Cl_2]/[O_2]$.

$$C_6H_5 + Cl_2 \rightarrow C_6H_5Cl + Cl \qquad (8)$$

$$C_6H_5 + O_2 + M \rightarrow C_6H_5O_2 + M \qquad (1)$$

Phenyl radicals were generated via the Cl atom initiated oxidation of benzaldehyde.

$$Cl_2 + h\nu(\lambda \geq 290 \text{ nm}) \rightarrow 2\ Cl \qquad (13)$$

$$Cl + C_6H_5CHO \rightarrow C_6H_5C(O) + HCl \qquad (14)$$

$$C_6H_5C(O) + Cl_2 \rightarrow C_6H_5C(O)Cl + Cl \qquad (15)$$

$$C_6H_5C(O) + O_2 + M \rightarrow C_6H_5C(O)O_2 + M \qquad (16)$$

$$C_6H_5C(O)O_2 + C_6H_5C(O)O_2 \rightarrow 2C_6H_5C(O)O + O_2 \qquad (17)$$

$$C_6H_5C(O)O \rightarrow C_6H_5 + CO_2 \qquad (18)$$

Experiments were performed at total pressures of 10−700 Torr of N_2 diluent with the concentration ratios $[Cl_2]/[O_2]$ of 0.028−0.124. Figure 8 shows typical IR spectra obtained before

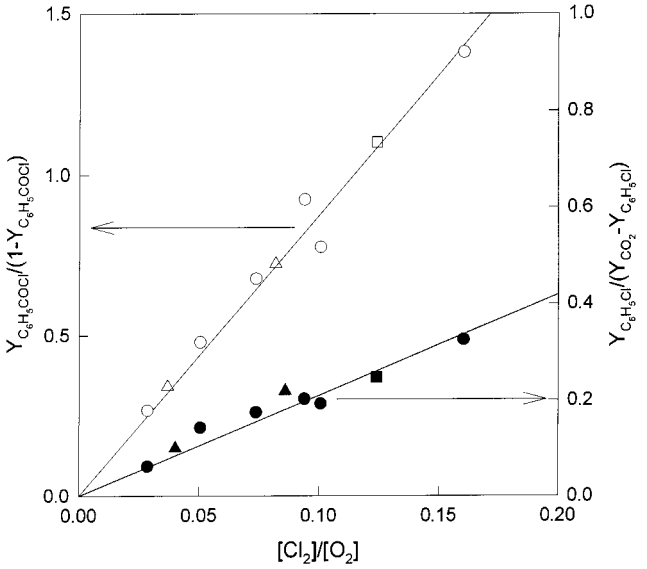

Figure 9. Plot of $Y_{C_6H_5C(O)Cl}/(1 - Y_{C_6H_5C(O)Cl})$ vs $[Cl_2]/[O_2]$ (open symbols) and $Y_{CO_2}/(Y_{CO_2} - Y_{C_6H_5Cl})$ vs $[Cl_2]/[O_2]$ (filled symbols) in experiments conducted at 700 (circles), 100 (squares), and 10 (triangles) Torr total pressure and 296 K. *Y* represents product molar yield.

(A) and after (B) a 7 s irradiation of a mixture of 9.92 mTorr C_6H_5CHO, 5.52 Torr O_2 and 557 mTorr Cl_2 in 700 Torr of N_2 at 296 K. Subtraction of features attributable to C_6H_5CHO from part B gives the product spectrum shown in part C. Comparison of the IR features in part C with reference spectra of $C_6H_5C(O)Cl$ and C_6H_5Cl in parts D and E shows the formation of these compounds.

The molar yield of C_6H_5Cl, $Y_{C_6H_5Cl}$, provides a measure of the importance of reaction 8 as a fate of phenyl radicals. The molar yield of CO_2, Y_{CO2}, provides a measure of the yield of phenyl radicals. Assuming that phenyl radicals are lost by reaction with either Cl_2 or O_2, then a plot of $Y_{C_6H_5Cl}/(Y_{CO_2} - Y_{C_6H_5Cl})$ versus $[Cl_2]/[O_2]$ should be linear, pass through origin, and have a slope $= k_8/k_1$. Using similar logic, a plot of $Y_{C_6H_5C(O)Cl}/(1 - Y_{C_6H_5C(O)Cl})$ should be linear, pass through origin, and have a slope $= k_{15}/k_{16}$.[48] Figure 9 shows a plot of $Y_{C_6H_5C(O)Cl}/(1 - Y_{C_6H_5C(O)Cl})$ versus $[Cl_2]/[O_2]$ for experiments conducted in 10, 100, or 700 Torr of N_2 diluent. By analogy to the reactions of other alkyl radicals with Cl_2, it is expected that the kinetics of reaction 8 will not be dependent on total pressure. As seen from Figure 9, there was no observable effect of total pressure over the range studied suggesting that reaction 1 is at or near the high-pressure limit for total pressures >10 Torr of N_2 diluent. Linear least-squares analysis of the data in Figure 9 give $k_8/k_1 = 2.1 \pm 0.4$ and $k_{15}/k_{16} = 8.7 \pm 1.8$. Quoted errors include two standard deviations from the regression analysis and uncertainties associated with the reference spectra. The value of k_{15}/k_{16} is consistent with that reported previously.[48] Combining $k_8/k_1 = 2.1 \pm 0.4$ with $k_8 = (2.96 \pm 0.53) \times 10^{-11}$ (see section 3.3) gives $k_1 = (1.4 \pm 0.4)$ x 10^{-11} cm^3 molecule^{-1} s^{-1}.

There have been three previous measurements of k_1 in the gas phase. Preidel and Zellner[8] monitored the phenyl radical using absorption at 488 nm following the photolysis of C_6H_5Cl in the presence of O_2 and derived an upper limit of $k_1 < 2.0 \times 10^{-17}$ cm^3 molecule^{-1} s^{-1}. As discussed in section 3.3, it is now understood that phenyl radicals do not absorb at the monitoring wavelength employed by Preidel and Zellner[8] and their value for k_1 does not need to be considered further. Yu and Lin conducted two studies of k_1. In their first study the loss of phenyl radicals in the presence of O_2 was monitored at 504.8 nm and a value of $k_1 = (3.87 \pm 0.43) \times 10^{-15}$ cm^3 molecule^{-1} s^{-1} was derived.[10] In their second study it was found that absorption by $C_6H_5O_2$ radicals was substantial at 504.8 nm and that this interference led to a significant underestimation of k_1.[11] By monitoring the rate of formation of $C_6H_5O_2$ radicals using its absorption at 496.4 nm, a value of $k_1 = (1.81 \pm 0.11) \times 10^{-11}$ cm^3 molecule^{-1} s^{-1} was derived in 40 Torr of Ar at 297 K.[11] The result from the present work, $k_1 = (1.4 \pm 0.4) \times 10^{-11}$ cm^3 molecule^{-1} s^{-1}, is in agreement with that reported by Yu and Lin[11] and with that observed in the aqueous phase.[49] The consistency between the values of k_1 derived from monitoring the rise of absorption at 496.4 nm in real time over a period of approximately 1 ms[11] and by the FTIR relative rate methods herein over much longer time scales (minutes) show that the peroxy radical $C_6H_5O_2$ formed in reaction 1 is a stable species.

4. Conclusions

We report herein the first absolute measurement of the visible absorption spectrum of the phenyl radical in the region 490−535 nm. The absorption cross sections reported here will facilitate quantification of phenyl radicals in future spectroscopic studies. Rate data concerning the reactions of phenyl radicals with Cl, Br, and Cl_2 are measured for the first time. At ambient temperature and pressure the reaction of phenyl radicals with O_2 is shown to proceed with a rate constant $k_1 = (1.4 \pm 0.4) \times 10^{-11}$ cm^3 molecule^{-1} s^{-1}. In one atmosphere of air the lifetime of phenyl radicals with respect to addition of O_2 to give $C_6H_5O_2$ radicals is approximately 1.4×10^{-8} s. Further studies are needed to elucidate the atmospheric fate of $C_6H_5O_2$ radicals.

Acknowledgment. This work is supported in part by a Grant-in-Aid from the Ministry of Education, Science, Sports and Culture (No. 13640502 and priority field "Radical Chain Reactions") and Sumitomo Foundation. We thank Ole John Nielsen (Copenhagen University) and Askar Fahr (National Institute for Standards and Technology) for helpful discussions.

References and Notes

(1) Marshall, E. L.; Owen, K., Ed. *Motor Gasoline*; Royal Society of Chemistry: London (ISBN no. 0-85404-409-4).
(2) Farrell, J. T. ExxonMobil Research and Engineering Company. Private communication. 2002.
(3) Calvert, J. G.; Atkinson, R.; Becker, K. H.; Kamens, R. M.; Seinfeld, J. H.; Wallington, T. J.; Yarwood, G. *Mechanisms of Atmospheric Oxidation of Aromatic Hydrocarbons*; Oxford University Press: New York, 2002.
(4) Marinov, N. M.; Pitz, W. J.; Westbrook, C. K.; Vincitore, A. M.; Castaldi, M. J.; Senkan, S. M.; Melius, C. F. *Combust. Flame* **1998**, *114*, 192.
(5) Porter, G.; Ward, B. *Proc. R. Soc. London* **1965**, *287*, 457.
(6) Cercek, B.; Kongshang, M. *J. Phys. Chem.* **1970**, *74*, 4319.
(7) Ikeda, N.; Nakashima, N.; Yoshihara, K. *J. Am. Chem. Phys.* **1985**, *107*, 3381.
(8) Preidel, M.; Zellner, R. *Ber. Bunsen-Ges. Phys. Chem.* **1989**, *93*, 1417.
(9) Gunion, R. F.; Gilles, M. K.; Polak, M. L.; Lineberger, W. C. *Int. J. Mass Spectrom. Ion Processes* **1992**, *115*, 601.
(10) Yu. T.; Lin M. C. *J. Am. Chem. Soc.* **1993**, *115*, 4371.
(11) Yu. T.; Lin M. C. *J. Am. Chem. Soc.* **1994**, *116*, 9571.
(12) Yu. T.; Lin, M. C.; Melius, C. *Int. J. Chem. Kinet.* **1994**, *26*, 1095.
(13) Yu. T.; Lin, M. C. *J. Phys. Chem.* **1994**, *98*, 2105.
(14) Park, J.; Chakraborty, D.; Bhusari, D. M.; Lin. M. C. *J. Phys. Chem. A* **1999**, *103*, 4002.
(15) Park, J.; Burova, S.; Rodgers, A. S.; Lin. M. C. *J. Phys. Chem. A* **1999**, *103*, 9036.
(16) Choi, Y. M. Xia, W. S.; Lin. M. C. *J. Phys. Chem. A* **2000**, *104*, 7030.
(17) Wallington, T. J.; Egsgaard, H.; Nielsen, O.J.; Platz, J.; Sehested, J.; Stein, T. *Chem. Phys. Lett.* **1998**, *290*, 363.
(18) Houston, J.; Andrews, L.; Lund, P. A.; Schatz, P. N. *J. Chem. Phys.* **1980**, *73*, 4932.

(19) Radziszewski, J. G. *Chem. Phys. Lett.* **1999**, *301*, 565.
(20) Radziszewski, J. G.; Nimlos, M. R.; Winter, P. R.; Elloson, G. B. *J. Am. Chem. Soc.* **1996**, *118*, 7400.
(21) Hassanzadeh, P.; Miller, J. H. *J. Phys. Chem.* **1992**, *96*, 6570.
(22) Engert, J. M.; Dick, B. *Appl. Phys. B* **1996**, *63*, 531.
(23) Miller, J. H.; Andrews, L.; Lund, P. A.; Schatz, P. N., *J. Chem. Phys*. **1980**, *73*, 4932.
(24) Pacansky, J.; Brown, D. W. *J. Phys. Chem.* **1983**, *87*, 1553.
(25) Johnson, R. P. *J. Org. Chem.* **1984**, *49*, 4857.
(26) Krauss. M.; Roszak, S. *J. Mol. Struct. (THEOCHEM)* **1994**, *310*, 155.
(27) O'Keefe, A.; Deacon, D. A. *Rev. Sci. Instrum.* **1988**, *59*, 2544.
(28) Tonokura, K.; Koshi, M. *J. Phys. Chem.* **2000**, *104*, 8456.
(29) Ninomiya, Y.; Hashimoto, S.; Kawasaki, M.; Wallington, T. J. *Int. J. Chem. Kinet.* **2000**, *32*, 125.
(30) Tanaka, J. *Nippon Kagaku Zasshi* **1958**, *79*, 1114.
(31) Wallington, T. J.; Japar, S. M., *J. Atmos. Chem.* **1989**, *9*, 399.
(32) (a) Becke, A. D. *J. Chem. Phys.* **1993**, *98*, 5648. (b) Becke, A. D. *J. Chem. Phys.* **1992**, 96, 2155. (c) Becke, A. D. *J. Chem. Phys.* **1992**, *97*, 9173.
(33) Lee, C.; Yang, W.; Parr, R. G. *Phys. Rev. B* **1988**, *37*, 785.
(34) (a) Wong, M. W.; Dunning, T. H., Jr. *J. Chem. Phys.* **1993**, 98, 1358. (b) Kendall, R. A.; Dunning, T. H., Jr. *J. Chem. Phys.* **1992**, 96, 6796.
(35) Frisch, M. J.; Trucks, G. W.; Schlegel, H. B.; Scuseria, G. E.; Robb, M. A.; Cheeseman, J. R.; Zakrzewski, V. Z.; Montgomery, J. A., Jr.; Stratmann, R. E.; Burant, J. C.; Dapprich, S.; Millam, J. M.; Daniels, A. D.; Kudin, K. N.; Strain, M. C.; Farkas, O.; Tomasi, J.; Barone, V.; Cossi, M.; Cammi, R.; Mennucci, B.; Pomelli, C.; Adamo, C.; Clifford, S.; Ochterski, J.; Petersson, G. A.; Ayala, P. Y.; Cui, Q.; Morokuma, K.; Malick, D. K.; Rabuck, A. D.; Raghavachari, K.; Foresman, J. B.; Cioslowski, J.; Ortiz, J. V.; Baboul, A. G.; Stefanov, B. B.; Liu, G.; Liashenko, A.; Piskorz, P.; Komaromi, I.; Gomperts, R.; Martin, R. L.; Fox, D. J.; Keith, T.; Al-Laham, M. A.; Peng, C. Y.; Nanayakkara, A.; Gonzalez, C.; Challacombe, M.; Gill, P. M. W.; Johnson, B.; Chen, W.; Wong, M. W.; Andres, J. L.; Gonzalez, C.; Head-Gordon, M.; Replogle, E. S.; Pople, J. A. *Gaussian 98*, revision A.7; Gaussian, Inc.: Pittsburgh, PA, 1998.
(36) Nakashima, N.; Yoshihara, K. *Laser Chem.* **1987**, *7*, 177.
(37) Zauli, C. *Comput. Phys. Commun.* **1994**, *79*, 555.
(38) Absolute uncertainty is $\leq \pm 2$ cm^{-1}.
(39) Ichimura, T.; Mori, Y. *J. Chem. Phys.* **1973**, *58*, 288.
(40) Fahr, A.; Stein, S.E. *J. Phys. Chem.* **1988**, *92*, 4951.
(41) Louw, R.; Rothuizen, J. W.; Wegman, R. C. C. *J. Chem. Soc., Perkin Trans. 2*, **1973**, 1635
(42) Fahr, A.; Stein, S. E. *Symp. Int. Combust. Proc.* **1989**, *22*, 1023.
(43) Baulch, D. L.; Duxbury, J.; Grant, S. J.; Montague, D. C. *J. Phys. Chem. Ref. Data* **1981**, *10*, Suppl.
(44) Sokolov, O.; Hurley, M. D.; Wallington, T. J.; Kaiser, E. W.; Platz, J.; Nielsen, O. J.; Berho, F.; Rayez, M.-T.; Lesclaux, R. *J. Phys. Chem. A*, **1998**, *102*, 10671.
(45) Park, J.; Lin, M. C. *J. Phys. Chem. A* **1997**, *101*, 14.
(46) Scharping, H, Zetzsch, C. *J. Mol. Spectrosc.* **1985**, *112*, 8.
(47) Maric, D.; Burrows, J. P.; Meller, R.; Moortgat, G. K. *J. Photochem. Photobiol. A* **1993**, *70*, 205.
(48) Caralp, F.; Foucher, V.; Lesclaux, R.; Wallington, T. J.; Hurley, M. D. *Phys. Chem. Chem. Phys.* **1999**, *1*, 3509.
(49) Sommeling, P. M.; Mulder, P.; Louw, R.; Avila, D. V.; Lusztyk, J.; Ingold, K. U. *J. Phys. Chem.* **1993**, *97*, 8361.